https://doi.org/10.48048/tis.2024.7140

Effect of Gd and Ce Doped $BiFeO_3$ for Photocatalytic Activity

Beerelli Rajitha and R. Padma Suvarna*

Department of Physics, Jawaharlal Nehru Technological University Ananthapur, Ananthapuramu, India

(*Corresponding author's e-mail: padmajntua@gmail.com)

Received: 29 May 2023, Revised: 28 July 2023, Accepted: 8 September 2023, Published: 15 September 2023

Abstract

In this current research work deals with the synthesis, characterization and photocatalytic activity of gadolinium (Gd) and cerium (Ce) doped bismuth ferrite oxide $BiFeO_3$ (BFO). All the samples BFO, BGF-1, BGCF-1, BGCF-2 and BGCF-3 were synthesized by sol-gel method. The structural analysis carried out by X-ray diffraction (XRD), surface morphology examined by field emission scanning electron microscopy (FE-SEM) with EDAX and transmission electron microscopy (TEM), the magnetic properties investigated using vibration sample magnetometer (VSM) and their photocatalytic activity was evaluated by Rhodamine B (RhB) dye under visible light irradiation. The results found that the Gd (0.1 wt.%) and Ce doped (0.1 wt.%) BFO showed better photocatalytic activity as compared to BFO and other samples.

Keywords: BFO, Gadolinium and cerium, Sol-gel characterization, RhB dye, Photocatalytic activity

Introduction

Water pollution is a major issue in the globe today, causing serious health and environmental risks to both aquatic and human life [1,2]. Now a day's dyes are used in many fields, such as food, textile and many other industries. Since the majority of dyes are poisonous, organic dye pollution is a pressing issue on a global scale that results in a lack of clean and healthy water [3]. Water with colored surfaces receives less sunlight, which inhibits the growth of biota and photosynthetic activity. RhB dye's high stability is advantageous for a variety of industrial applications, however because of its complex structure, decolorization is a challenging process [4,5]. Industrial wastewater must be appropriately treated before being drained to reduce the risk of pollution from these harmful substances and to permit the recycling of water resources.

Photocatalytic degradation is potentially one of the inexpensive and most powerful techniques for controlling the current decontamination of water from dye pollutants at a large- scale. BFO has recently gained a lot of attention for photo-induced applications due to its comparatively less band gap (2.2 - 2.8 eV) compared to other materials. According to reports, doping Gd onto BFO results in increased photocatalytic degradation of RhB because of ferromagnetic behaviour [6,7]. In addition, the effects of Ce doping on the morphology and magnetic characteristics have been investigated [8-10]. It has been reported that the doping of rare-earth ions such as Gd and Ce onto BFO shows enhanced photocatalytic degradation of RhB [11-21]. In this report BFO and $Bi_{1-x}Gd_xFe_{1-y}Ce_yO_3$ (where x = 0.1 & y = 0.05, 0.1 and 0.15) samples were synthesized by sol-gel method. The enhanced photocatalytic properties of BFO and Gd&Ce doped BFO under visible light were observed and discussed.

Materials and methods

Materials

Iron (III) nitrate nanohydrate $Fe(NO_3)_3.9H_2O$, Nitric acid (HNO_3, 65 %), Bismuth (III) nitrate pentahydrate $Bi(NO_3)_3.5H_2O$, Cerium nitrate hexahydrate $Ce(NO_3)_3.6H_2O$, Gadolinium (III) nitrate hexahydrate $Gd(NO_3)_3.6H_2O$ and Tartaric acid ($C_4H_4O_6$). All the chemicals are analytical grade from Sigma Aldrich and were used for further purification.

Methods

The BFO, $Bi_{1-x}Gd_xFeO_3$ (x = 0.1 wt.%, as BGF-1) and $Bi_{1-x}Gd_xF_{1-y}Ce_yO_3$ (y = 0.05, 0.1 and 0.15 wt.%, as BGCF-1, BGCF-2, BGCF-3) samples were synthesized by sol-gel method. First, 1.91 gm of iron (III) nitrate nanohydrate $Fe(NO_3)_3.9H_2O$ dissolved in 50 mL of distilled water and 10 mL of nitric acid (HNO_3, 65 %) was added to the mixture to get the pH to 1. Following 2.42 gm of bismuth (III) nitrate pentahydrate $Bi(NO_3)_3.5H_2O$ added to the solution, the mixture was continually stirred until a clear solution had formed. Drop by drop 25 mL of tartaric acid (M = 1) added to the solution as a chelating agent. The light yellowish transparent solution is formed after the solution heated to 90 °C for 1 h while being continuously stirred to produce the gel. Next, the temperature was raised to 180 °C (or more) to promote solvent evaporation and powder creation. The dried powder was calcined at a temperature of 600 °C for 3 h and at the end fine powder in a brown color was produced.

In the similar method to prepare $Bi_{1-x}Gd_xFeO_3$ (x = 0.1 wt.%) and $Bi_{1-x}Gd_xF_{1-y}Ce_yO_3$ (y = 0.05, 0.1 and 0.15 wt.%) the stoichiometric amount of gadolinium (III) nitrate hexahydrate $Gd(NO_3)_3.6H_2O$, cerium nitrate hexahydrate $Ce(NO_3)_3.6H_2O$, iron (III) nitrate nanohydrate $Fe(NO_3)_3.9H_2O$, and bismuth (III) nitrate pentahydrate $Bi(NO_3)_3.5H_2O$ added and continuously stirred till the formation of powder with proper heat application.

Results and Discussion

Figure 1 shows the X-Ray diffraction pattern of BFO, Gd and Ce doped BFO samples. For pure BFO diffraction peaks are showed at 2θ = 22.4, 31.8, 32.0, 38.9, 39.5, 45.7, 51.4, 51.7, 56.4, 59.0, 66.3, 67.1, 70.6, 71.5, 76.0 ° the associated planes are displayed in **Figure 1(a)**. The sample is hexagonal with the R3c space group and can be classified in a single phase BFO for an angle between 2θ = 10 and 80 °. It is also well matched with JCPDS card no.86-1518 [22]. In the doping of Gd and Ce in BFO, the diffraction of the patterns was similar to that of the BFO. However, in all the doped samples a very slight amount of the $Bi_{24}FeO_{40}$ (represented with # in the **Figure 1**) related impurity phase can be observed at 2θ = 27.8 ° [23]. The effect of Gd and Ce the magnified XRD pattern around 2θ = 22 to 34 ° can be identified that the diffraction planes (104) and (110) are shifted towards a higher angle direction and 2 peaks are merged into a single peak, as well as (012) plane (2θ = 22.4 °) the intensity gradually decreased, which is indicated the phase transformation as shown in **Figure 1(b)**. In addition for BFO, BGF-1, BGCF-1, BGCF-2, and BGCF-3, the average crystalline size determined using Scheer's formula was found to be 19.9, 15.8, 14.4, 13.1 and 12.6 nm, respectively.

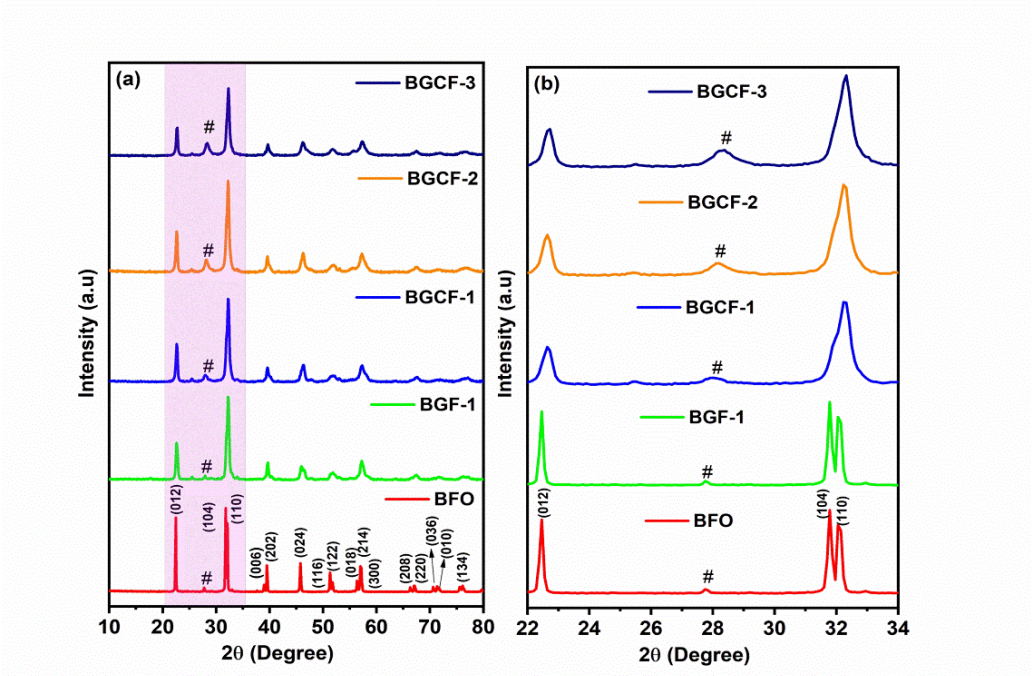

Figure 1 XRD spectra of (a) BFO, BGF-1, BGCF-1, BGCF-2 and BGCF-3, (b) Magnified view of XRD pattern angle 2θ = 22 to 34 °, for BFO, BGF-1, BGCF-1, BGCF-2 and BGCF-3 samples.

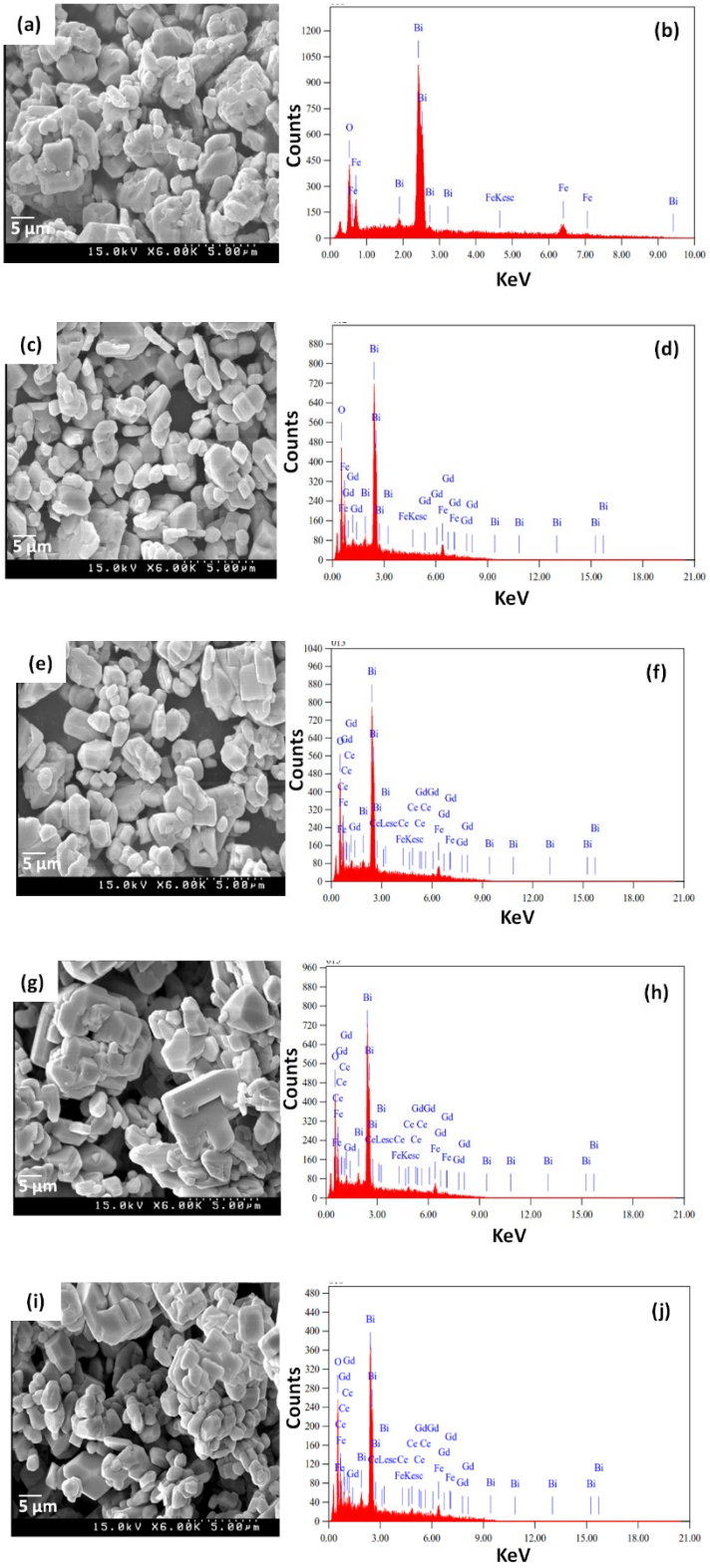

Figure 2 The FE-SEM and EDAX images; (a-b) BFO, (c-d) BGF-1, (e-f) BGCF-1, (g-h) BGCF-2, and (i-j) BGCF-3 samples.

Figures 2(a) - 2(j) shows the FE-SEM and EDAX images of BFO, BGF-1, BGCF-1, BGCF-2 and BGCF-3 respectively found with irregular clusters. According to the EDAX results, the doped samples contain the elements Bi, Fe, O, Gd, and Ce. In all doped samples the atoms content percentage of Gd

almost same and Ce slightly varied. It can be concluded that Gd and Ce ions were successfully doped into BFO samples. The morphological and dimensional changes in Gd and Ce doped BFO samples strongly depend on the doping wt.%.

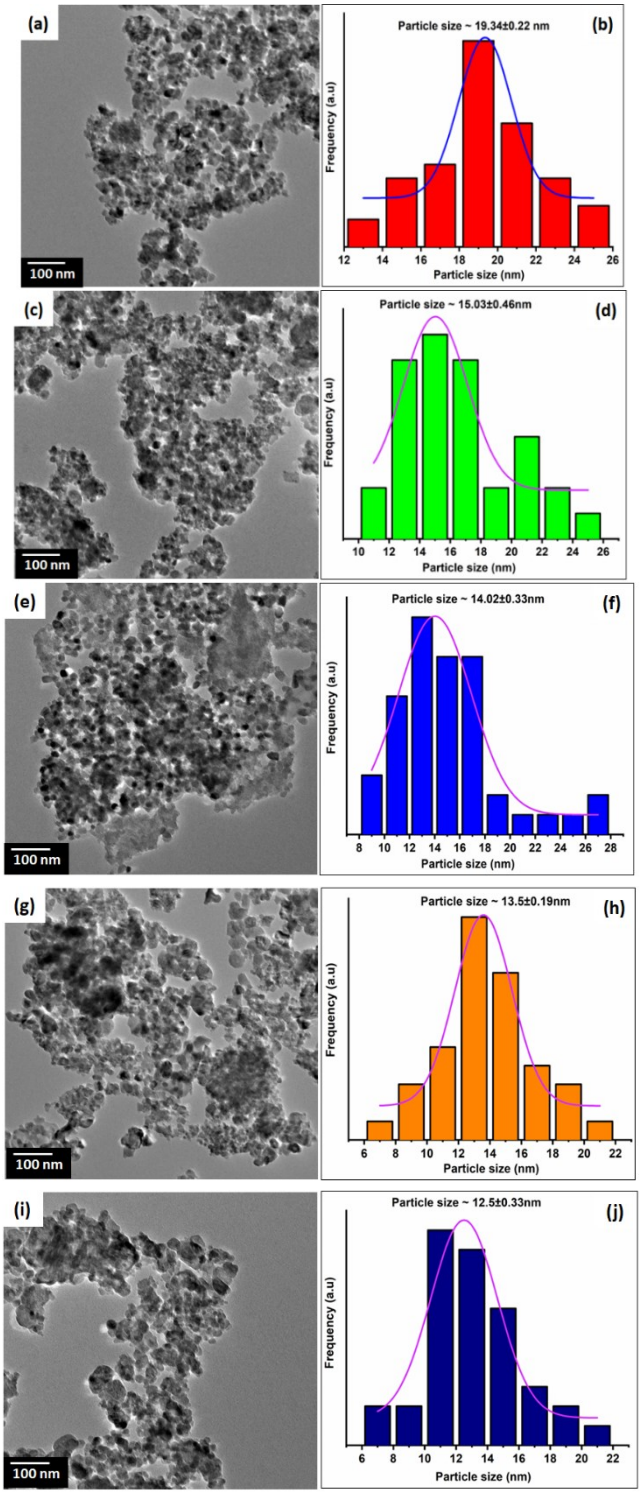

Figure 3 TEM images and particle size distribution of (a-b) BFO, (c-d) BGF-1, (e-f) BGCF-1, (g-h) BGCF-2, and (i-j) BGCF-3 samples.

TEM images reveal the agglomerated and spherical symmetry with the average particle size estimated in the range of 12 to 19 nm for BFO, BGF-1, BGCF-1, BGCF-2, and BGCF-3 as shown in

Figures 3(a) - 3(j) and it is in good agreement with the crystalize size derived from the XRD results. The average particle size is found to decrease with Gd and Ce doping. Thus we can conclude that the substitution of rare-earth in BFO is accompanied by a significant decrease of particle size [24].

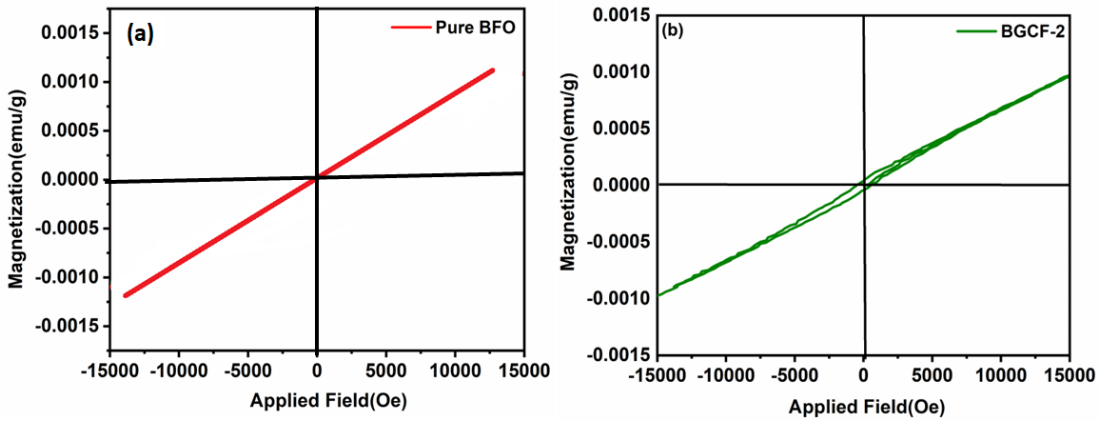

Figure 4 Room temperature M - H curves of (a) BFO, (b) BGCF-2 samples.

The Ferromagnetic hysterisis curve for pure BFO and BGCF-2 sample was measured at room temperature. If the prepared sample possesses magnetic particles, it can be separated by using the applied magnetic field. The magnetization hysteresis (M - H) curves of BFO and BGCF-2 samples are displayed in **Figure 4(a)-4(b)**. Because of impurities present in BFO weak magnetism was observed as per the **Figure 4(a)** [25-30]. Due to the breaking of crystal symmetry brought on by the addition of Gd and Ce into BFO, and the small spontaneous magnetization observed for BGCF-2 sample **Figure 4(b)**. Doping might have raised the canting angle, which would have improved the magnetic characteristics.

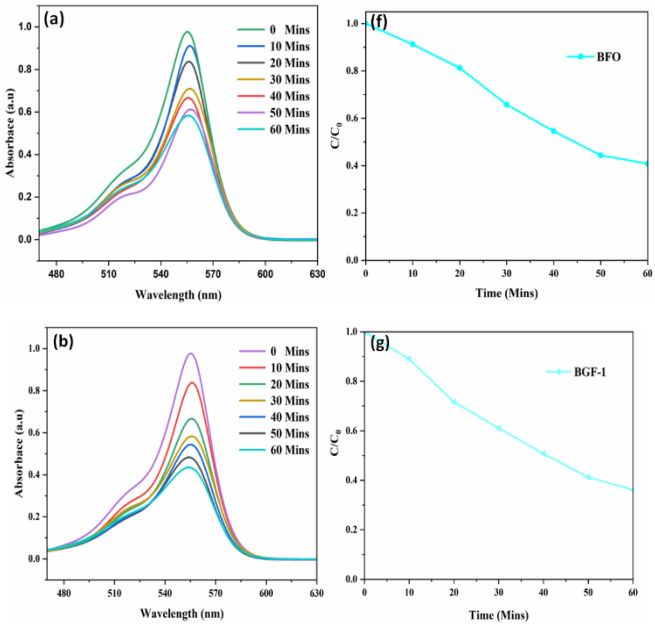

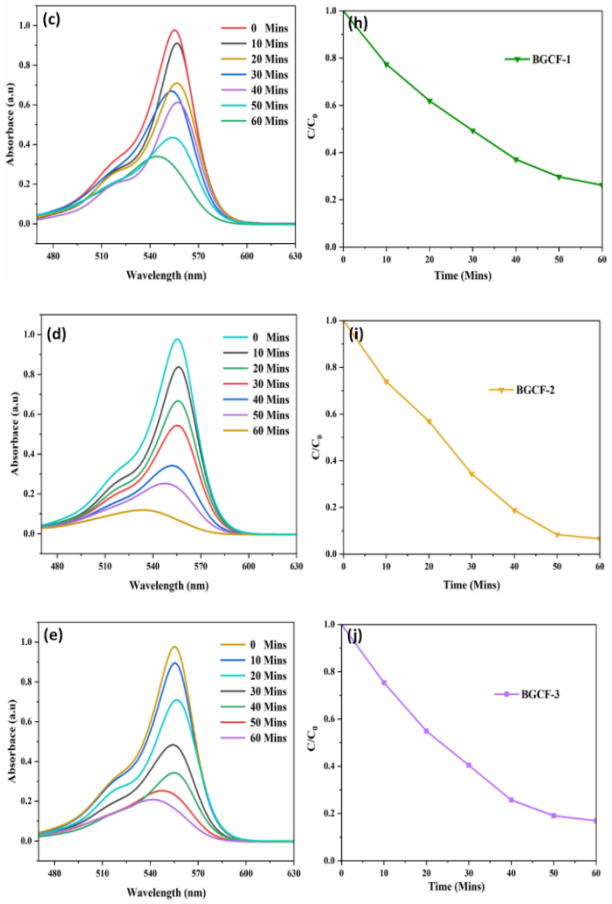

Figure 5 Absorption spectra and photocatalytic degradation efficiencies of RhB dye; (a-j) BFO, BGF-1, BGCF-1, BGCF-2, and BGCF-3 samples.

The photocatalytic activity of BFO, BGF-1, BGCF-1, BGCF-2 and BGCF-3 samples were evaluated by degradation of the typical organic contaminate RhB dye under visible light irradiation and time-dependent photodegradation of RhB is illustrated in **Figures 5(a)** - **5(e)** and their degradation constants from **Figures 5(f)** - **5(j)** in 60 min. Typically, 50 mg photo-catalyst powder was dispersed into 100 mL of the 10 ppm Rhodamine B dye solution which was prepared from the stock solution and stirred in the dark for 2 h to reach the adsorption-desorption equilibrium between the photo-catalyst and organic dye molecules. Further, the same procedure was carried out using visible light irradiation for all considered samples with continuous stirring and a small amount of samples were collected with equal time intervals of up to 60 min.

It is believed that the photocatalytic activity is largely dependent on the generation, separation, transport and recombination of photogenerated electron-hole pairs in the photocatalysis process. Compare to BFO, the BGF and BGCF reduces charge recombination, resulting in a longer lifetime of photogenerated electron-hole pairs. The surface barrier rises as Gd and Ce dopant concentration approach the optimal value, making the space charge area narrower and e^-, h^+ pair separation inside the region more effective. The space-charge area gets much narrower and the incident light penetrates deeper into the sample when the Gd and Ce dopant concentration is higher than its optimal level. As a result, in these conditions, it is simpler for the e^-,h^+ pairs to recombine, which reduces the photocatalytic activities. In this regard, the doped BFO samples must be at a certain level for the greatest photocatalytic activity. Up to a specific amount of catalyst such as Gd-0.1 and Ce-0.1, it has been shown that the rate of degradation increases as the amount of catalyst increases. The reaction rate becomes almost constant after this point. This phenomenon could be explained by the fact that as catalyst concentration increases, the amount of the catalyst's exposed surface area will also rise. Since the catalyst was entirely covering the bottom of the reaction vessel, the rate of reaction increased as a result. However, if the amount of catalyst is increased over a certain point, just the thickness of the layer (and not the exposed surface area) would grow and it could be effect on degradation time.

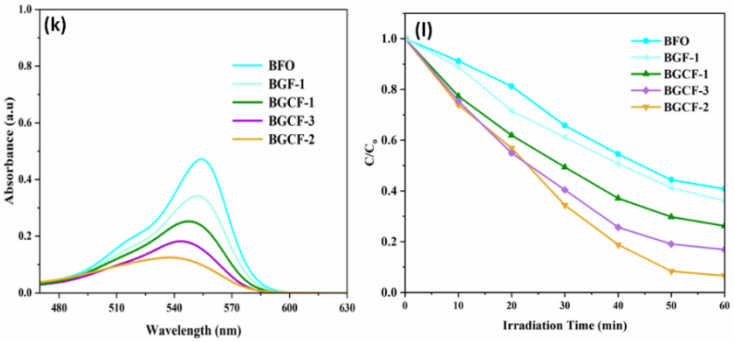

Figures 5(k) - 5(l) Champion results of absorption spectra and photocatalytic degradation efficiencies of RhB dye for BFO, BGF-1, BGCF-1, BGCF-2, and BGCF-3 samples.

Figures 5(k) - 5(l) shows photocatalytic activity & degradation constant (C/C_0) for the BFO and Gd & Ce doped BFO. From **Figure 5(k)** we can say that the degradation of Rhodamine B for the sample BFO is about 50 % and for BGCF-2 is very high that is almost 90 %. It is also observed from the **Figure 5(l)** that BGCF-2 shows the highest degradation rate constant compare to all other samples for the time 60 min. Finally, among all the prepared samples, the BGCF-2 contributes significantly highest photocatalytic activity.

Conclusions

In summary, $BiFeO_3$, $Bi_{1-x}Gd_xFeO_3$ (x = 0.1 wt.%) and $Bi_{1-x}Gd_xF_{1-y}Ce_yO_3$ (y = 0.05, 0.1 and 0.15 wt.%) samples were successfully synthesized by sol-gel method and their structural, surface morphology and magnetic properties investigated. The photocatalyst activity was done by Rhodamine B (RhB) dye under visible light irradiation. The results found that, the photocatalytic degradation performance of BGCF-2 sample improved significantly in comparing BFO and other BGF-1, BGCF-1 and BGCF-3 samples i.e., BGCF-2 showed almost double dye degradation effect with compare to BFO.

Acknowledgements

The author is thankful to Centre for Nano Science & Technology, University of Engineering Science & Technology, India, JNTU Hyderabad & University of Hyderabad in India & Osmania University in India for providing lab and instrumentation facility.

References

[1] MA Iqbal, SI Ali, F Amin, A Tariq, MZ Iqbal and S Rizwan. La- and Mn-Codoped bismuth Ferrite/Ti_3C_2 MXene composites for efficient photocatalytic degradation of congo red dye. *ACS Omega* 2019; **4**, 8661-8.

[2] S Khan and A Malik. Toxicity evaluation of textile efuents and role of native soil bacterium in biodegradation of a textile dye. *Environ. Sci. Pollut.* 2018; **25**, 4446-58.

[3] N Vijayakumar, SK Venkatraman, S Imthiaz, EA Drweesh, MM Elnagar, S Koppala and S Swamiappan. Synthesis and characterization of calcium and magnesium based oxides and titanates for photocatalytic degradation of rhodamine B: A comparative study. *Sci. Rep.* 2023; **13**, 3615.

[4] X Xiao, M Xiao-Lin, L Zhao-Ying, L Wen-Wei, H Yuan, M Xiao-Bo, L Li-Xia and Y Han-Qing. Degradation of rhodamine B in a novel bio-photoelectric reductive system composed of *Shewanella oneidensis* MR-1 and Ag_3PO_4. *Environ. Int.* 2019; **126**, 560-7.

[5] GV Sree, P Nagaraaj, K Kalanidhi, CA Aswathy and P Rajasekaran. Calcium oxide a sustainable photocatalyst derived from eggshell for efficient photo-degradation of organic pollutants. *J. Cleaner Prod.* 2020; **270**, 122294.

[6] S Irfan, S Rizwan, S Yang, L Li and SB Asfandiyar. The Gadolinium (Gd^{3+}) and Tin (Sn^{4+}) Co-doped $BiFeO_3$ nanoparticles as new solar light active photocatalyst. *Sci. Rep.* 2017; **7**, 42493.

[7] RB Purusottam, H Cui, MC Sekhar, SVP Vattikuti, Y Suh and SH Park. Influence of Gd doping on the visible-light photocatalytic activity and magnetic properties of $BiFeO_3$ particles. *Mater. Res. Express* 2019; **6**, 115044.

[8] R Guo, L Fang, W Dong, F Zheng and M Shen. Enhanced photocatalytic activity and ferromagnetism in Gd doped $BiFeO_3$ nanoparticles. *J. Phys. Chem. C* 2010; **114**, 21390-6.
[9] M Sobhan, Q Xu, J Zhao, A Franklin, Y Hu, JS Tse and P Wu. Modification of surface chemistry by lattice Sn doping in $BiFeO_3$ nanofibers. *Europhys. Lett.* 2015; **111**, 18005-10.
[10] Q Yang, Q Xu, M Sobhan, Q Ke, F Anariba, KP Ong and P Wu. Simultaneous reduction in leakage current and enhancement in magnetic in $BiFeO_3$ nanofibers via optimized Sn doping. *Phys. Status Solidi Rapid Res. Lett.* 2014; **8**, 653-7.
[11] NSA Satar, R Adnan, HL Lee, RH Simon, T Kobayashi, MHM Kassim and NHM Kaus. Facile green synthesis of ytrium-doped $BiFeO_3$ with highly efficient photocatalytic degradation towards methylene blue. *Ceram. Int.* 2019; **44**, 19512.
[12] B Rajitha, KV Rao and PR Suvarna. Synthesis of multiferroic $BiFeO_3$ microcrystals for photocatalytic activity and stability performance. *Mater. Today Proc.* 2019; **26**, 126-9.
[13] BP Reddy, MC Sekhar, BP Prakash, Y Suh and SH Park Photocatalytic, magnetic, and electrochemical properties of La doped $BiFeO_3$ nanoparticles. *Ceram. Int.* 2018; **44**, 19512-21.
[14] R Mahesh, E Sagar, PV Reddy. A study of ferroelectric and magnetic properties of Rare Earth (RE = La, Nd, Sm, Gd) doped $BiFeO_3$ using modified becke johnson potential with SOC techniques. *Mater. Chem. Phys.* 2019; **232**, 460.
[15] D-Y Lin, H-Z Chen, M-C Kao and PL Zhang. Ferroelectric and electrical properties optimization of Mg-doped $BiFeO_3$ flexible multiferroic films. *Summetry* 2020; **12**, 1173.
[16] B Rajitha,V Rajendar and RP Suvarna. Influence of rare earth (Gd) and transition (Cu) doping in bismuth ferrite for photocatalytic activity and stability performance, Available at: https://doi.org/10.21203/rs.3.rs-3099139/v1
[17] Y Yang, L Kang and H Li. Enhancement of photocatalytic hydrogen production of $BiFeO_3$ by Gd^{3+} doping. *Ceram. Int.* 2019; **45**, 8017-22.
[18] N Zhang, D Chen, F Niu, S Wang, Q Laishun and H Yuexiang. Enhanced visible light photocatalytic activity of Gd-doped $BiFeO_3$ nanoparticles and mechanism insight. *Sci. Rep.* 2016; **6**, 26467.
[19] Z Chen, Y Wu, X Wang, W Jin and C Zhu. Ferromagnetism and enhanced photocatalytic activity in Nd doped $BiFeO_3$ nanopowders. *J. Mater. Sci. Mater. Electron.* 2015; **26**, 9929-40.
[20] H Maleki, M Zakeri and R Fathi. Experimental study of the effect of yttrium on the structural, thermal, and magnetic properties of $BiFeO_3$. *Appl. Phys. A* 2018; **124**, 728.
[21] ME Graf, SD Napoli, MA Barral, LMS Medina, RM Negri, M Sepliarsky and AM Llois. Rhombohedral *R*3*c* toorthorhombic *Pnma* phase transition induced by Y-doping in $BiFeO_3$. *J. Phys. Condens. Matter.* 2018; **30**, 285701.
[22] EMS Ghahfarokhi, K Helfi and ZM Shoushtari. Synthesis of the single-phase bismuth ferrite ($BiFeO_3$) nanoparticle and investigation of their structural, magnetic, optical and photocatalytic properties. *Adv. J. Chem. A* 2022; **5**, 45-58.
[23] G Wang, D Cheng, T He, Y Hu, Q Deng, Y Mao and S Wang. Enhanced visible-light responsive photocatalytic activity of $Bi_{25}FeO_{40}/Bi_2Fe_4O_9$ composites and mechanism investigation. *J. Mater. Sci. Mater. Electron.* 2019; **30**, 10923-33.
[24] P Rozina, PS Sawadh and K Sachin. Enhanced multiferroic properties in Cerium doped $BiFeO_3$. *Int. J. Adv. Sci. Tech. Res.* 2015; **5**, 138-44.
[25] Y Wang, Z Guo, Q Jia, J Dong, J Zhang and D Chen. Effect of Nd/Mn substitution on the structure and magnetic properties of nano- $BiFeO_3$. *J. Alloy. Comp.* 2019; **786**, 385-93.
[26] H Wang, C Yang, J Lu, W Meimei, S Jie, L Kuo, Z Junrong, L Guobao, J Tounan, K Takashi, L Fuhui, L Jianhua and W Yicheng. On the structure of α- $BiFeO_3$. *Inorg. Chem.* 2013; **52**, 2388-92.
[27] A Perejón, E Gil-González, PE Sánchez-Jiménez, JM Criado, and LA Pérez-Maqueda. Structural, optical, and electrical characterization of yttrium-substituted $BiFeO_3$ ceramics prepared by mechanical activation. *Inorg. Chem.* 2015; **54**, 9876-84.
[28] SV Kiselev, RP Ozerov and GS Zhdanov.Detection of magnetic arrangement in the $BiFeO_3$ ferroelectric by means of neutron diffraction study. *Doklady Akademii Nauk SSSR* 1962; **145**, 1255-8.
[29] F Zhang, X Zeng, D Bi, K Guo, Y Yao and S Lu. Dielectric, ferroelectric, and magnetic properties of Sm-doped $BiFeO_3$ ceramics prepared by a modified solid-state-reaction method. *Materials* 2018; **11**, 2208.
[30] S Mohanty and R Choudhary. Dielectric and electrical properties of $BiFeO_3$−$LiTaO_3$ systems. *J. Electron. Mater.* 2015; **44**, 2359-68.